Astronomy & Astrophysics manuscript no. ms
August 25, 2009

Peering through the veil: near-infrared photometry and extinction for the Galactic nuclear star cluster

Accurate near infrared H, Ks, and L' photometry and the near-infrard extinction-law toward the central parsec of the Galaxy

R. Schoedel[1], F. Najarro[2], A. Eckart[3], and K. Muzic[3]

[1] Instituto de Astrofísica de Andalucía (CSIC), C/ Camino Bajo de Huétor 50, 18008 Granada, Spain
e-mail: rainer@iaa.es
[2] Centro de Astrobiología (CSICINTA), Instituto Nacional de Técnica Aeroespacial, Ctra de Torrejón a Ajalvir, km 4, 28850 Torrejón de Ardoz, Madrid, Spain
e-mail: najarro@damir.iem.cisc.es
[3] I. Physikalisches Institut, Universität zu Köln, Zülpicher Strasse 77, 50937 Köln, Germany
e-mail: eckart@ph1.uni-koeln.de

;;

ABSTRACT

Context. The nuclear star cluster of the Galaxy is an important template for understanding its extragalactic counterparts, which can currently not be resolved into individual stars. Important drawbacks of observations of the Galactic center are, however, the presence of strong and spatially highly variable interstellar extinction and extreme crowding of the sources, which makes the use of adaptive optics techniques necessary. Both points pose serious obstacles to precise photometry that is needed for analyzing the stellar population.
Aims. The aims of this work are to provide accurate photometry in multiple near-infrared broadband filters, to determine the power-law index of the extinction-law toward the central parsec of the Galaxy, to provide measurements of the absolute extinction toward the Galactic center, and finally to measure the spatial variability of extinction on arcsecond scales.
Methods. We use observations of the central parsec of the Milky Way that were obtained with the near-infrared camera and adaptive optics system NAOS/CONICA at the ESO VLT unit telescope 4. The photometric method takes into account anisoplanatic effects and limits the corresponding systematic uncertainties to $\lesssim 2\%$. Absolute values for the extinction in the H, Ks, and L'-bands as well as of the power-law index of the near-infrared extinction-law are based on the well-known properties of red clump stars. Extinction maps are derived based on $H - Ks$ and $Ks - L'$ colors.
Results. We present Ks-band photometry and additionally photometry in the H and/or L'-bands for $\sim$ 7700 stars. An extinction map for the Galactic center is presented. Both its statistical and systematic uncertainties are estimated to be $< 10\%$. Extinction is found to vary significantly on arcsecond scales, with a mean value of $A_{Ks} = 2.74 \pm 0.30$ mag. From a number of recent publications we compute a weighted mean distance of the Galactic center of $R_0 = 8.04 \pm 0.16$ kpc, which has an uncertainty of just 2%. Based on this R_0 and on the RC method, we derive absolute mean extinction values toward the central parsec of the Galaxy of $A_H = 4.56 \pm 0.12$ mag, $A_{Ks} = 2.52 \pm 0.12$ mag, and $A_{L'} = 1.24 \pm 0.18$ mag. We estimate values of the power-law indices of the extinction-law of $\alpha_{H-Ks} = 2.22 \pm 0.23$ and $\alpha_{Ks-L'} = 1.38 \pm 0.29$. Mean extinction values in a circular region with 0.5" radius centered on Sagittarius A* are $A_{H,SgrA*} = 4.34 \pm 0.11$, $A_{Ks,SgrA*} = 2.45 \pm 0.03$, and $A_{L',SgrA*} = 1.24 \pm 0.08$.

1. Introduction

Nuclear star clusters (NSCs) are located at the photometric and dynamical centers of almost all spiral galaxies. They have only been discovered via *HST* observations in the 1990s, but are of great interest because they are the densest and most massive clusters in their host galaxies. Frequently they contain supermassive black holes at their centers. They show signs of recurring star formation, and the discovery of rotation of the NSCs of NGC 4244 (Seth et al. 2008) and of the Milky Way (Trippe et al. 2008; Schoedel et al. 2009) indicates that NSCs may at least partially form by accretion of material from their host galaxy. A concise review of the properties of NSCs and hypotheses on their formation is given in Böker (2008).

Studying the NSC at the Galactic center (GC) is of great importance for the understanding of NSCs in general because in the next decades it will remain impossible to resolve any but the brightest individual stars in extragalactic NSCs, even with 50m-class telescopes. A further reason for the importance of the GC NSC is that the existence of the supermassive black hole, Sagittarius A*, at the GC is well established and the mass of this black hole has been determined with high precision (e.g., Ghez et al. 2008; Gillessen et al. 2009). Strong interest in the stellar population at the GC was raised by spectroscopic observations, which have revealed the existence of numerous massive, young stars within 0.5 pc of Sagittarius A*. Those young stars are witnesses of a starburst event that occurred about 4 million years ago. The young stars are arranged in a non-isotropic pattern and at least 50% of them are located in a rotating disk (see Bartko et al. 2009; Lu et al. 2009).

Unfortunately, there are two important drawbacks in observational studies of the Milky Way's NSC: extreme crowding and high extinction. While the great progress made in adaptive optics techniques at 8-10m-class telescopes in the past years has been

highly successful in reducing the problem of crowding, it nevertheless remains a serious issue. Even with instruments such as NACO at the ESO VLT, strong crowding limits the point-source sensitivity within ~ 0.5 pc of Sagittarius A* so significantly that only stars more massive than $\sim 2\,M_{\odot}$ can be detected in this region. This means that we can still detect only of the order 10% of the stars in the NSC (Schödel et al. 2007a). Additionally, it is notoriously difficult to extract accurate photometric measurements from AO observations of crowded fields, particularly when the field-of-view exceeds the size of the isoplanatic angle.

As concerns extinction, we can consider ourselves lucky that we can observe the GC at all. Within 2-3 pc of Sagittarius A* there exist plenty of clouds that are almost or completely opaque even in the near-infrared (for example, see Fig. 1 in Schödel et al. 2007a). Average extinction toward the central parsec in the K-band reaches $A_K \approx 3$. As concerns extinction at visual wavelengths, Rieke & Lebofsky (1985) found $A_V/A_K \sim 9$, but more recent studies indicate higher values of $A_V/A_K \sim 16$ (Nishiyama et al. 2008), or even $A_V/A_K \sim 29$ (Gosling et al. 2009). Therefore, the stellar population at the GC becomes observable only at near-infrared wavelengths. Only the brightest stars can be seen in the J-band. Reasonable S/N on the stars is only reached in the H, K, and L bands. This restriction to a tight wavelength window, where most stars show only small color indices, combined with the fact that the extinction toward the GC is not only high, but also variable on small spatial scales of a few arcseconds (Gosling et al. 2006; Schödel et al. 2007a), makes photometric studies of the stellar population at the GC extremely difficult.

Although adaptive optics assisted integral field spectroscopy has resulted in the classification of hundreds of stars within ~ 0.5 pc of Sagittarius A* (e.g., Maness et al. 2007; Paumard et al. 2006), this technique is extremely time consuming in both observations and data analysis. In order to efficiently probe large fields in the Galactic center for the presence of young, massive stars, it is therefore desirable to improve the photometric observations in a way that enables us to at least crudely distinguish whether a star in the GC is of early or of late spectral type. How this can be done in spite of the difficulties described above has been demonstrated recently by Buchholz et al. (2009). They used intermediate band filters across the K-band, calibrated photometry locally with the help of red clump stars, and used the CO bandhead absorption feature of late-type stars as a distinguishing criterion.

Accurate knowledge of extinction has impact in many different aspects of GC research: the stellar surface number density s not only a function of distance from Sagittarius A*, but is also strongly dependent on local extinction (Schödel et al. 2007a); extinction is an important ingredient for modeling stellar atmospheres (e.g., Najarro et al. 1997a; Martins et al. 2007a); extinction in the infrared is also important for estimating the intrinsic brightness of the near-infrared emission from the accretion flow or outflow related to Sagittarius A* (e.g., Genzel et al. 2003; Eckart et al. 2006; Do et al. 2009). The mentioned examples show that one must know not only the absolute value of extinction, but also how it changes as a function of wavelength and how it varies on spatial scales as small as one to a few arcseconds.

Until just about a decade ago, the extinction law from near- to mid-infrared wavelengths ($\sim 1 - 8\,\mu$m) was thought to be described well by a "universal" power-law, $A_\lambda \propto \lambda^{-\alpha}$, with a power-law index of $\alpha = 1.75$ (e.g., Draine 1989). First doubts on this model were shed by spectroscopic observations of the GC with ISO SWS that showed clear deviations from this model at wavelengths $\gtrsim 3\,\mu$m (Lutz et al. 1996). Subsequent studies have confirmed that the near- to mid-infrared extinction-law is more complex than a simple power-law. While it seems well established by now that a simple power-law is an adequate description of the wavelength dependence of extinction in the near-infrared, albeit with a stronger wavelength dependence as previously thought, the situation is less clear longward of $\sim 3\,\mu$m. Recent ivestigation shows that the extinction law decreases much less rapidly at $\lambda > 3\,\mu$m than suggestd by earlier estimates and may actually be almost constant at $5 - 10\,\mu$m (see Nishiyama et al. 2009, for an extensive discussion of these points). Taking the problem even a step further, in a recent study of extinction toward the nuclear bulge Gosling et al. (2009) find that the index of the power-law extinction-law can change on spatial scales as small as 5 arcseconds. This signifies that we may be forced to abandon the concept of a universal extinction-law.

It is evident that the topic of extinction toward the central parsec of the Galaxy needs to be re-visited. Extinction maps for the central 0.5-1 pc were recently presented by Schödel et al. (2007a) and (Buchholz et al. 2009). However, these papers were not mainly focused on extinction and the extinction maps were rather side-products. Both papers used the old $A_\lambda \propto \lambda^{-1.75}$ extinction-law (Draine 1989). Neither the extinction law not absolute extinction were examined in depth. Also, the absolute photometric calibration in our previous works was of limited accuracy because the PSF for the stars was either truncated (Schödel et al. 2007a) or because complex local calibration procedures had to be adopted (Buchholz et al. 2009).

The aim of this paper is to carry us a step forward in observational studies of the GC NSC by addressing two of the above described problems: accurate photometry with AO over a large FOV and accurate measurements of extinction. Schoedel (submitted to A&A) has recently presented a method for the photometric analysis of AO data with spatially variable PSF, but a very limited number of suitable PSF reference stars. Based on this method, in this paper we analyze imaging observations of the GC in the H, Ks, and L' bands and provide accurate photometry (with both statistical and systematic uncertainties of the order $\sim 5\%$ at Ks) for several thousand sources observed in these bands within $\sim$1 pc of Sagittarius A*. We determine both the absolute extinction and the extinction law at the various bands and provide a detailed extinction map (resolution of 1" – 2") for the central parsec of the GC.

2. Observations

The observations used in this work were obtained with the near-infrared camera and adaptive optics (AO) system NAOS/CONICA (short NACO) at the ESO VLT unit telescope 4 [1]. The Ks $\approx 6.5 - 7.0$ supergiant IRS 7 was used to close the loop of the AO, using the NIR wavefront sensor. The sky background was measured on a largely empty patch of sky, a dark cloud about 400″ north and 713″ east of the target. Sky subtraction, bad pixel correction, and flat fielding were applied to the individual exposures. The NACO S27 camera, with a pixel scale of 0.027″/pix, was used for both H and Ks band observations. The field-of-view (FOV) of a single exposure is thus $28'' \times 28''$. The observations were dithered by applying a rectangular dither pattern with the center of the dithered exposures positioned approximately at (8.0″, −2.6″), (−6.1″, −2.7″), (−6.1″, 11.2″),

[1] Based on observations made with ESO Telescopes at the La Silla or Paranal Observatories under programmes ID 077.B-0014 and 081.B-0648

and (8.1″, 11.3″) east and north of Sgr A*. In the text we refer to these four offsets as dither positions 1, 2, 3, and 4. The combined FOV of the observations is about 40″ × 40″ and is offset to the north with respect to Sgr A* because the guide star IRS 7 is located about 5.6″ north of Sgr A*.

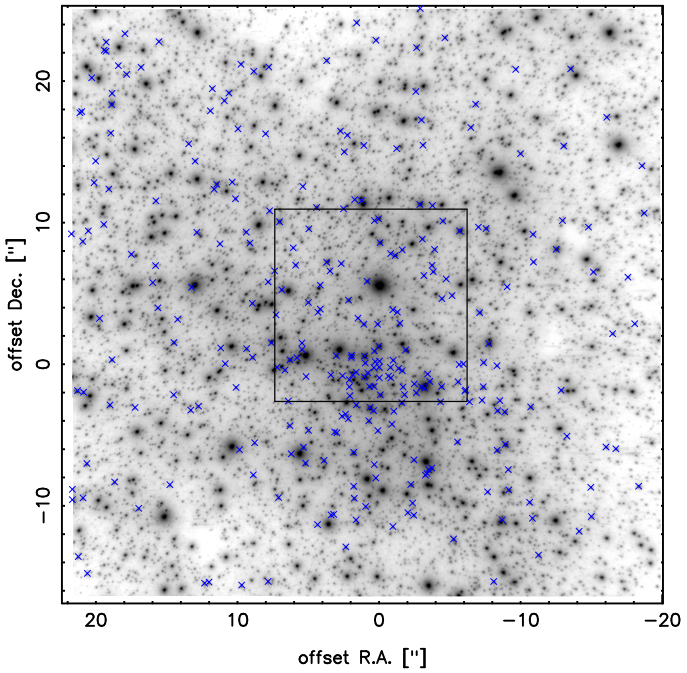

Fig. 1. Mosaic image of the Ks-band observations. North is up and east is to the left. Offsets are given in arcseconds from Sgr A*. The guide star, IRS 7, is the brightest star within the rectangle, about 5.5" north of Sgr A*. The black rectangle indicates the area of overlap between the 4 dither positions. Blue crosses mark early-type stars identified by their $H - Ks$ colors with extinction/reddening correction applied (see section 5 and Fig. 8).

Seeing ranged between 0.6" and 1.0" for both H and Ks observations. Sky transparency variations were below 1% during the observations. The achieved Strehl ratio ranged between ∼ 20% (∼ 15%) near the guide star and ∼ 8% (∼ 8%) at 25" distance from the guide star in the Ks-(H-)band. The Strehl ratio was estimated using the *Strehl* algorithm of the ESO *eclipse* software package (Devillard 1997) on PSFs extracted at various positions in the image. From the multiple measurements we estimate the 1 σ uncertainty of the measured Strehl ratio to ∼ 3%. Table 1 summarizes the observations. The detector integration time (DIT) was set to 2.0 s in order to avoid saturation of the brightest stars. The central pixels of a smll number of the brightest stars were saturated in Ks. Their cores were repaired using nearby unsaturated stars and the PSF extraction routine of *StarFinder*. After 28 DITs, the instrument averaged the data to a single exposure (NDIT= 28). In this way, 8 individual exposures were obtained per dither position. The exposures of each respective dither position were aligned (to compensate for small residual shifts) with the *jitter* algorithm of the ESO *eclipse* software package (Devillard 1997). We show the combined FOV of the Ks-band observations in Fig. 1. Note that the photometry and astrometry in this work was done on the combined images of *each dither position* and *not on the combined mosaic* of all images (as shown in Fig. 1) in order to have a constant signal-to-noise ratio over the entire images. The ∼ 13.5" × 13.5" overlap area between the four dither positions is indicated by the rectangle in Fig. 1.

Table 1. Details of the imaging observations used in this work. DIT is the detector integration time, NDIT is the number of integrations that were averaged on-line by the read-out electronics, N is the number of individually recorded exposures. The total integration time of each observation amounts to N×NDIT×DIT. The pixel scale of all observations is 0.027″ per pixel.

Date	$\lambda_{\rm central}$ [μm]	$\Delta\lambda$ [μm]	N	NDIT	DIT [s]
29 April 2006	1.66	0.33	32	28	2
29 April 2006	2.18	0.35	32	28	2
26 May 2008	3.80	0.62	202	150	0.2

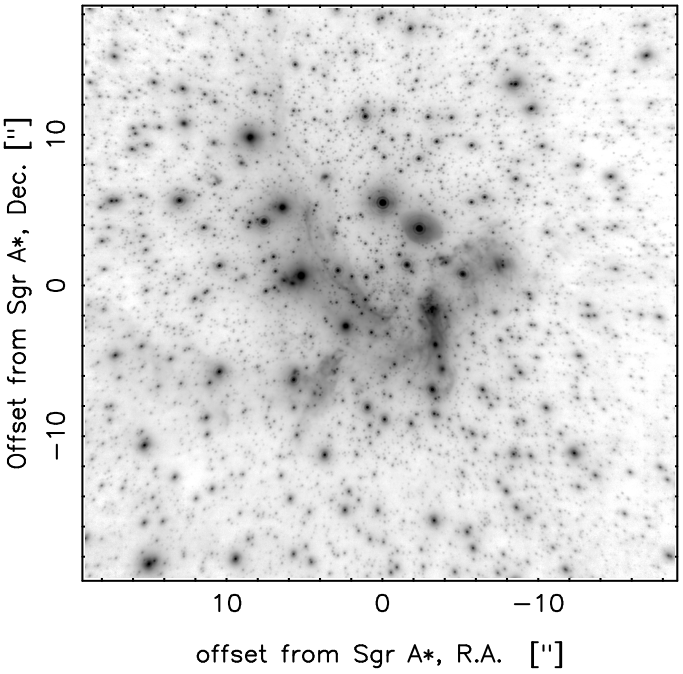

Fig. 2. Mosaic image of the L'-band observations. North is up and east is to the left. Offsets are given in arcseconds from Sgr A*.

Seeing ranged between 1.0" and 2.0" for the L' observations. Sky transparency variations were below 1%. The observations were random jittered, with a jitter box width of 20". Offsets by 60" in random directions were alternated with observations of the target. The frames taken on the offsets frames, where the stellar density is lower, were used to construct sky frames. The 7 offset frames nearest in time to a given exposure on the target were median combined and subtracted as sky measurement. Flat fielding and bad pixel correction were applied. Finally, all exposures were combined with the *jitter* algorithm of the ESO *eclipse* software package. The resulting mosaic image is shown in Fig. 2.

3. Photometry

Due to the extreme source density at the GC aperture photometry cannot be applied accurately to GC imaging data. Therefore PSF fitting techniques must be used. In AO imaging anisoplanatic effects can lead to a systematic bias in the photometry of point sources when PSF fitting is used for estimating the flux of the stars. This bias depend on various factors such as distance

from the guide star, observing wavelength, and atmospheric conditions at the time of the observations. In case of the H-band data used in this work the systematic error of the photometry can reach 0.25 mag across the FOV, if a single, non-variale PSF is used (see Schoedel, submitted to A&A). For example, anisoplanatic effects make stars at distances larger than the isoplanatic angle appear elongated, with their major axes pointing toward the guide star. This can be nicely seen in the image shown in Fig. 2 (note: usually anisoplanatic effects are stronger at shorter wavelengths, but in the observations used for this paper, it happens that those effects are stronger in the L'-band than in the Ks-band image). Various methods for dealing with anisoplanatic effects have been suggested. A straightforward and effective method to deal with anisoplanatic effects is presented in a companion paper (Schoedel, submitted to A & A). It not only provides accurate point source photometry but also reliable estimation of the diffuse background emission. In brief, the method consists of two steps: (a) Wiener deconvolution, using a point spread function (PSF) extracted from the guide star (or bright stars near the guide star), in this case IRS 7; (b) photometry and astrometry on the deconvolved image via PSF fitting with the *StarFinder* (Diolaiti et al. 2000) program package. The image is partitioned into overlapping sub-frames that are smaller than the isoplanatic angle. Those sub-frames are analyzed independently. As shown in Schoedel (submitted to A&A) this method minimizes the systematic uncertainty of the point source photometry due to anisoplanatic effects to $\lesssim 0.02$ mag across the 28" $\times$ 28" FOV of the images at each dither position.

After deconvolution with PSFs extracted from IRS 7, the H- and Ks-band images from the four dither positions were partitioned into 13×13 overlapping sub-images of 256×256 pixel^2 ($\sim$ 6.9" $\times$ 6.9"). The shifts between sub-images were thus just 64 pixels in x- and/or y-direction to assure large overlap between the sub-frames. We used the following *StarFinder* parameters: *min_corr* = 0.9, *thresh* = [5., 5.], and *back_box* = 30. In order to avoid spurious detections, point source detectino was also run on non-deconvolved images and only sources that were discovered in both the deconvolved and non-deconvolved images were included in the final list of detected stars. The images for the diffuse background and residuals were obtained by recombining the corresponding sub-frames. The method provides two kinds of uncertainties for the photometric and astrometric measurements: *formal* uncertainties, computed by the *StarFinder* algorithm from Gaussian and photon noise, and *PSF uncertainties*, resulting from incomplete knowledge of the local PSF. The latter is calculated by comparing multiple measurements of the stars because they are present in several sub-frames. For stars without multiple measurements we adopted a PSF uncertainty of 0.02 mag for the H-band and 0.015 mag for the Ks-band (see Fig. 3). The results of multiple measurements were averaged. Since deconvolution changes the noise properties of the image, the formal uncertainties computed by *StarFinder* are too small (see Schoedel, submitted to A& A, for details). Monte Carlo simulations were used to determine a correction factor with which we scaled the formal uncertainties. The final uncertainties were calculated by quadratically combining the re-scaled formal fit uncertainties with the PSF uncertainties. The data in the overlap region between the four dither positions were averaged. Stars present in the overlap region between the dithered fields in the H and Ks observations were used to check the photometric accuracy. Photometry on the stars in the overlapping fields shows that the uncertainties estimated by the our method are correct (see Schoedel, submitted to A&A).

Photometry on the L' image was performed in a very similar way, except that there was only one combined frame to be examined. The PSF for initial linear deconvolution was extracted from IRS 7. The size of the sub-frames for local PSF fitting was 300×300 pixel^2, with a shift of 50 pixels between the frames. Since the L' data are very rich in structure as concerns the diffuse emission, we set the *back_box* to a smaller value (20 pixels).

Zero points for the NACO instrument for various combinations of cameras, filters, and dichroics (that split the light between wavefront sensor and camera) are determined routinely within the ESO instrument calibration plan. Zero points for all filters used in this work and for the corresponding setup (camera S27, dichroic N20C80) were determined via observation of a standard star during the same night as the observations: $ZP_H = 23.64 \pm 0.05$, $ZP_{Ks} = 22.85 \pm 0.05$, and $ZP_{L'} = 22.38 \pm 0.15$. Additional uncertainty of the zero point is caused by the uncertainty of the PSF that is used for deconvolution. From experiments (choosing different PSF sizes) we estimate this additional uncertainty to $\lesssim 0.03$ mag. We combine this additional uncertainty quadratically with the previous uncertainty and obtain final zero point uncertainties of $\Delta ZP_H = 0.06$, $\Delta ZP_{Ks} = 0.06$, and $\Delta ZP_{L'} = 0.15$.

Plots of photometric uncertainty vs. magnitude for all point sources discovered in the individual bands are shown in Fig. 3. We combined the photometric results to a final list, requiring that each star must be detected in at least two different bands. The final lists of detected point sources was aligned with the coordinate system of the Ks-observations. The full list of all stars and their fluxes in the different bands is given in Table A.2, available online.

4. Constraining extinction with the red clump

Color-magnitude diagrams of our data are shown in Fig. 4. The densely populated area around $Ks \approx 15.6$ and $L' \approx 14.2$ is due to red clump (RC) stars, which are the equivalent to horizontal branch stars in metal-rich populations. The luminosities and colors of RC stars are narrowly distributed and are only weakly dependent on age and metallicity, particularly for clusters older than $\sim$1.6 Gyr (e.g., Castellani et al. 1992; Alves 2000a; Grocholski & Sarajedini 2002).

The H, Ks, and L' luminosity functions (LFs) are shown in the bottom panel of Fig. 4. The RC feature is clearly visible as a bump in all LFs. We fitted all LFs with the combination of exponentials plus Gaussians. The locations of the peaks of the RC as derived from these fits are $H_{\rm RC} = 17.58 \pm 0.016$, $Ks_{\rm RC} = 15.57 \pm 0.009$, and $L'_{\rm RC} = 14.22 \pm 0.008$. The uncertainties of the fits are significantly smaller than the uncertainty of the absolute photometric calibration (0.06 mag for H and Ks, and 0.15 mag for L'). Therefore we adopt the latter as uncertainties for the peak brightness of the RC in the three bands.

Since RC stars can be found in large numbers toward the Galactic bulge and center, they are highly useful for studying Galactic extinction and structure (e.g., Wozniak & Stanek 1996; Udalski 2003; Sumi 2004; Nishiyama et al. 2005, 2006a,b). The absolute magnitude of RC stars has been estimated to $M_K = -1.54 \pm 0.04$ (in the 2MASS system) by Groenewegen (2008) and to $M_K = -1.61 \pm 0.03$ by Alves (2000b). Both values are based on the *Hipparcos* catalogue. Here we adopt the more recent value for M_K. The difference between the K and Ks-magnitude is $\approx$ 0.01 mag (see discussion in Nishiyama et al. 2006b). Nishiyama et al. (2006b) estimated the distance to the

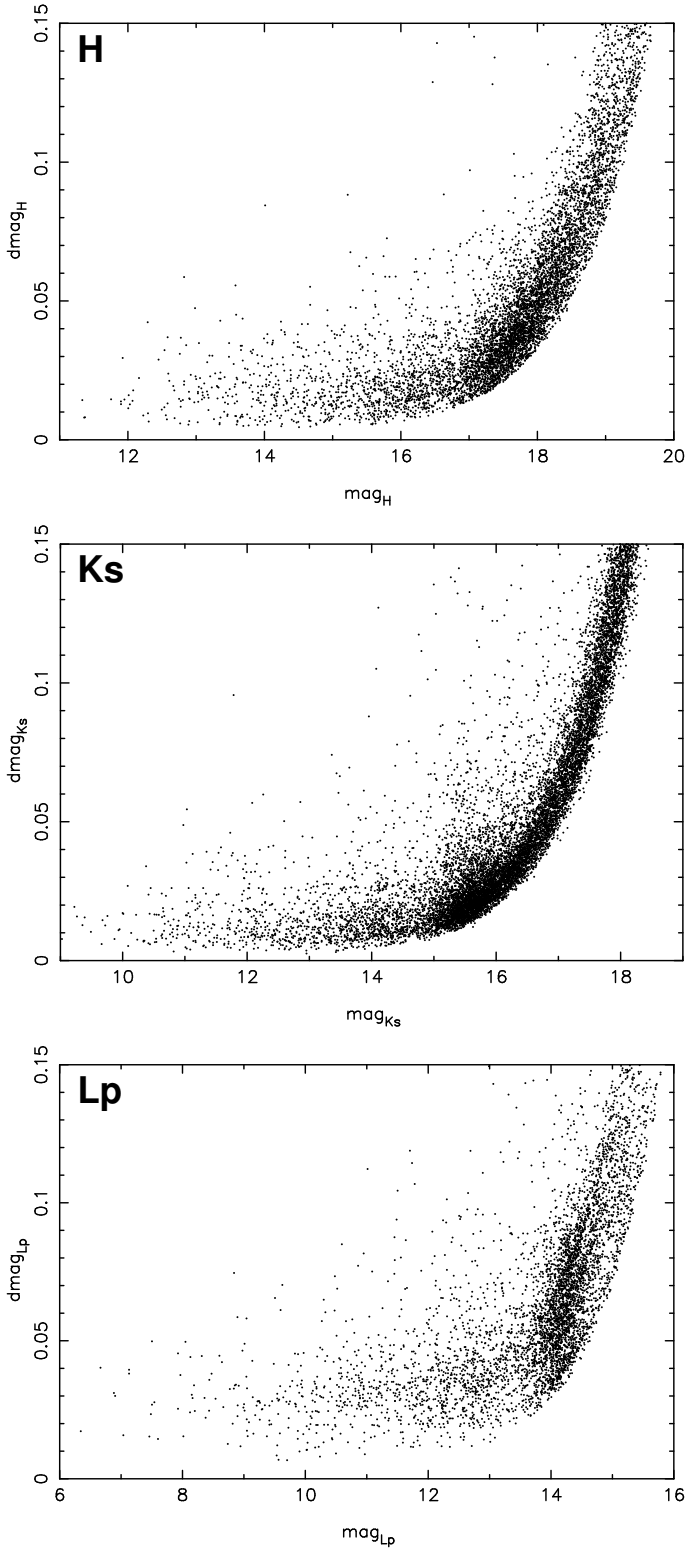

Fig. 3. Statistical photometric uncertainty vs. magnitude for the H- (top), Ks- (middle), and L'- (bottom) bands.

GC based on photometry of RC stars, calculating the distance modulus as

$$(m - M)_0 = Ks_{\mathrm{RC,intr.}} - M_{Ks} + \Delta M_K, \quad (1)$$

where $Ks_{\mathrm{RC,intr.}}$ is the intrinsic, reddening free magnitude of RC stars, M_{Ks} is their absolute Ks-magnitude, and ΔM_K the population correction for M_{Ks}. We adopt the same values as Nishiyama

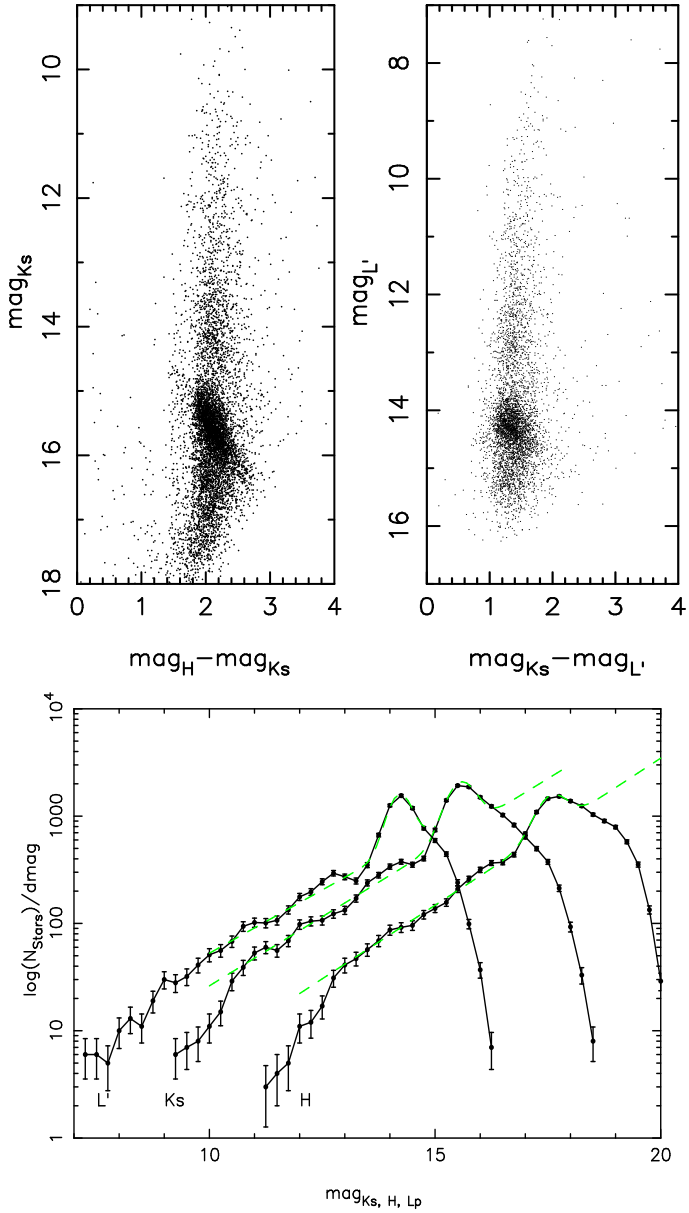

Fig. 4. Top: Color-magnitude diagrams; left: Ks vs. $H - Ks$; right: L' vs. $Ks - L'$. Bottom: L', Ks, and H luminosity functions. The dashed green lines are fits with an exponential plus a Gaussian.

et al. (2006b) for $\Delta M_K = -0.07$ and use $M_{Ks} = -1.54$ (see above). By assuming a GC distance, we can use the above equation to estimate the reddening free magnitude of RC stars. By comparing it subsequently with the magnitude of the RC clump peak as inferred from the luminosity function, we can then obtain an estimate of the absolute extinction in Ks toward the GC.

Numerous efforts to determine the distance of the GC have been made recently: 7.52 ± 0.36 kpc (Nishiyama et al. 2006b), 8.33 ± 0.35 kpc (Gillessen et al. 2009), 8.0 ± 0.6 kpc (Ghez et al. 2008), 7.94±0.45 kpc (Groenewegen et al. 2008), 8.07±0.35 kpc (Trippe et al. 2008), 8.4 ± 0.6 kpc (Reid et al. 2009), and 8.24 ± 0.6 kpc (Matsunaga et al. 2009). These distance estimates are based on different data sets and different methods and can be considered independent measurements. It appears therefore justified to combine these measurements to a weighted mean of $R_0 = 8.04 \pm 0.16$ kpc. This corresponds to a distance modulus of 14.52 ± 0.04. This simple exercise demonstrates that - under

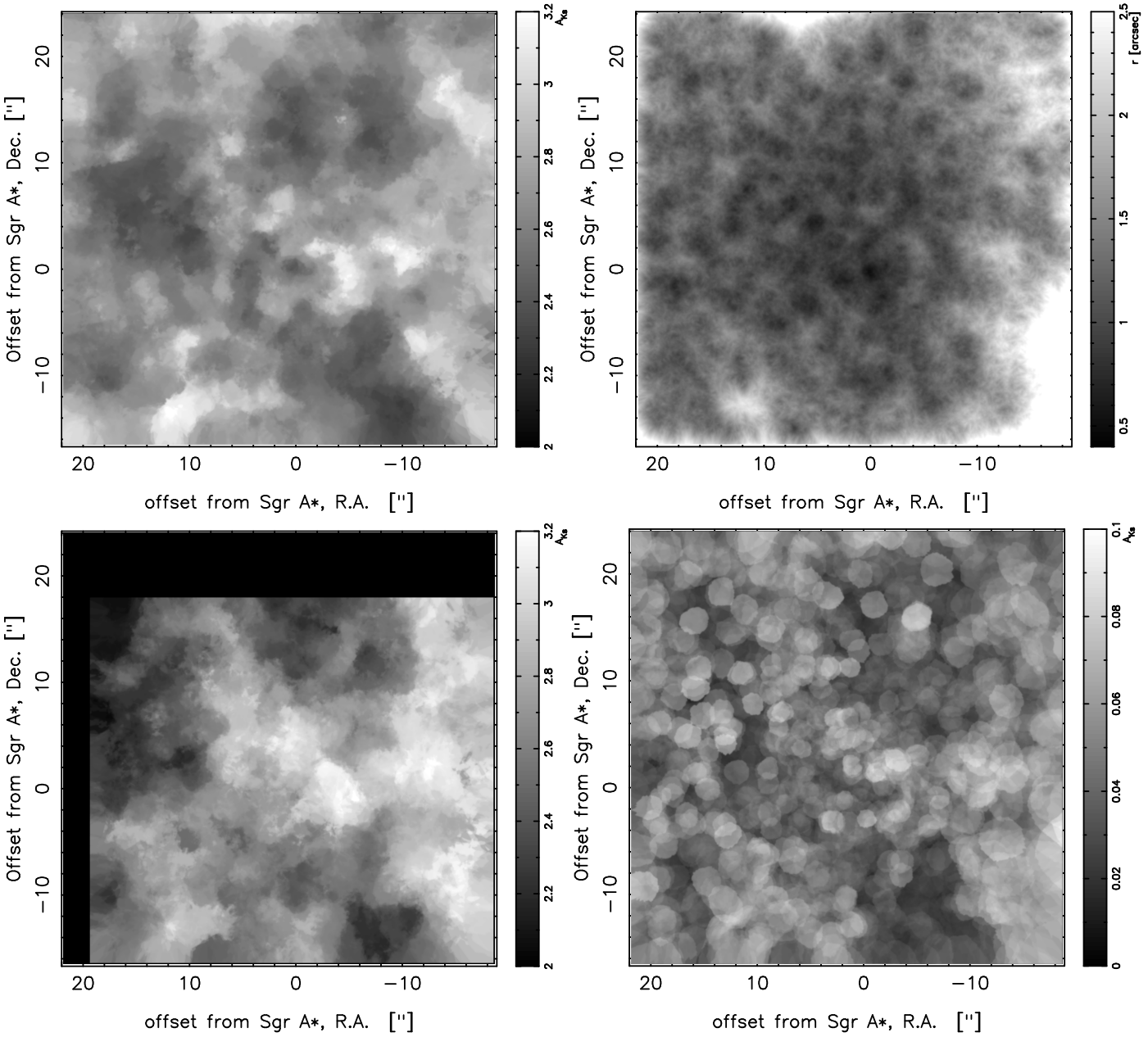

Fig. 6. Top left: Map of A_{Ks} for the GC derived from $H-Ks$ colors. Top right: Map of the resolution of the extinction, i.e. the radius in arcseconds at each position within which the 20 stars for the given measurement were detected. Bottom left: Map of A_{Ks} for the GC derived from $Ks-L'$ colors. Bottom right: Map of the statistical uncertainty of A_{Ks}, corresponding to the extinction map shown top left.

the assumption that these measurements are indeed statistically independent- R_0 is already known with the surprisingly small uncertainty of just 2%. Using this value we obtain a reddening free magnitude of the RC bump at the GC of $Ks_{\rm RC,intr.} = 13.05 \pm 0.09$. All uncertainties have been quadratically combined, with the uncertainty of R_0 bing the dominant contribution (0.04 mag).

The fit of the RC bump in the KsLF with a Gaussian (plus an exponential to fit the underlying luminosity function) results in $Ks_{\rm RC} = 15.57 \pm 0.06$. From the difference with the theoretical reddening free magnitude of the RC bump, this results in an average extinction of $A_{Ks} = 2.52 \pm 0.12$ toward the GC.

Assuming $H-Ks = 0.07 \pm 0.03$ and $Ks-L' = 0.07 \pm 0.03$ for the RC stars, we obtain in the same way estimates for $A_H = 4.46 \pm 0.12$ and $A_{L'} = 1.24 \pm 0.18$. Note that these values depend only on the well-known properties of RC stars and on the GC distance. They are independent of any assumptions on the extinction-law.

Assuming the validity of a power-law for the extinction law between H and Ks and between Ks and L', respectively (see, e.g., Nishiyama et al. 2009), we can derive form the above measurements the respective power-law indices $\alpha_{H-Ks} = 2.22 \pm 0.23$ and $\alpha_{Ks-L'} = 1.38 \pm 0.29$. Here the uncertainties include the uncertainties of the effective wavelengths of the corresponding bands. The effective wavelengths adopted in this work are $\lambda_{\rm eff,H} = 1.677 \pm 0.018\,\mu$m, $\lambda_{\rm eff,Ks} = 2.168\,pm0.012\,\mu$m, and $\lambda_{\rm eff,L'} = 3.636 \pm 0.012\,\mu$m. Details on how they have been calculated are given in appendix A.

As can be seen in the color-magnitude diagram shown in Fig. 4 (top left) there is a clear dependency of the Ks peak magnitude of the RC feature on $H-Ks$. Because of the narrow intrinsic distribution of colors and magnitudes of the RC stars we

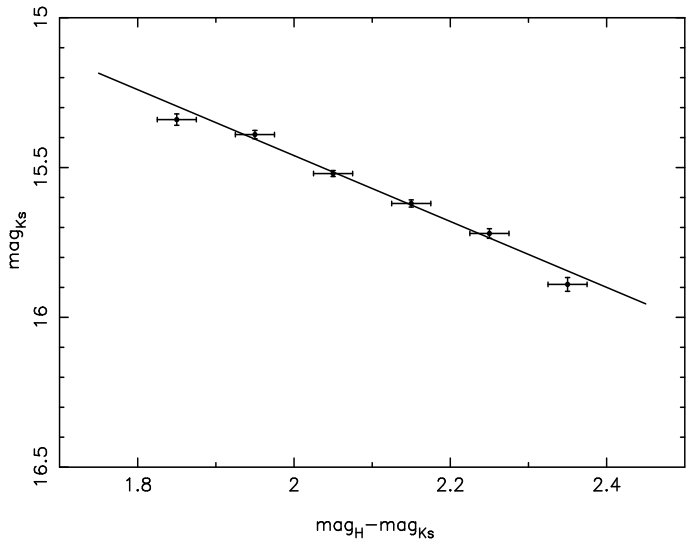

Fig. 5. Peak Ks-magnitude vs. $H-Ks$ color of the red clump.

expect this trend to be almost exclusively due to differential extinction. In order to quantify this relation, we extracted the KsLF in narrow ranges of $H-Ks$. The peaks of the RC features were then fitted with a Gaussian. This method is very similar to the one applied by Nishiyama et al. (2006a), who examined the location of the RC feature in different fields toward the GC in order to derive the reddening law. Figure 5 shows the thus measured RC Ks peak magnitude vs. $H-Ks$ along with a linear fit. Assuming $A_\lambda \propto \lambda^{-\alpha_{H-Ks}}$, the slope of the line gives $\alpha_{H-Ks} = 2.54 \pm 0.15$. As can be seen in the upper right panel of Fig. 4, there is no such clear trend of the RC visible in the plot of L' vs. $Ks-L'$. This is mainly because the number of stars measured in L' is smaller (smaller FOV) and because the range spanned by the $Ks-L'$ colors is limited due to the weak extinction in L' . We can therefore not apply this method to determine $\alpha_{Ks-L'}$ (see below for a different method, however).

5. An extinction map for the GC

We produced an extinction map for the FOV of the H and Ks observations of the GC by using the median of the $H-Ks$ colors of the 20 nearest stars at each position. Although the intrinsic colors of almost all stellar types are small at these wavelengths and therefore dominated by extinction, we tried to improve the estimates by applying a 0th order correction for intrinsic stellar colors. Stars fainter than $Ks = 14.5$ were assigned $(H-Ks)_0 = 0.07$ and stars brighter than this value were assigned $(H-Ks)_0 = 0.2$. Known early-type stars (taken from Buchholz et al. 2009) were assigned $(H-Ks)_0 = -0.03$. In order to assign these intrinsic colors, we used the GC distance, extinction, and the magnitude of the stars to roughly guess their type (see, e.g., Table 3 in Buchholz et al. 2009) and assigned colors from tables 7.6 and 7.7 in Cox (2000).

The map of $H-Ks$ colors was converted to an extinction map by assuming a power-law extinction-law with an index $\alpha_{H-Ks} = 2.22 \pm 0.32$ for the effective wavelengths of $\lambda_H = 1.677 \pm 0.012\,\mu$m and $\lambda_{Ks} = 2.168 \pm 0.012\,\mu$m. The uncertainty of these three parameters combined with the uncertainty of the photometric zero points results in a combined systematic uncertainty of $\sim 8.5\%$ on the calculated values of A_{Ks}. The extinction map based on $H-Ks$ colors is shown in the top left panel of Fig. 6. The top right panel of this figure shows the resolution of the extinction map, i.e. the radius at each position within which 20 stars were detected. The statistical uncertainty of the extinction at each point in the map is shown in the bottom right panel of Fig. 6. It is < 0.1 mag for the entire map. As a cross-check, we also created an extinction map based on $Ks-L'$ colors, in a completely analogous way. It is presented in the bottom left panel of Fig. 6 and shows the same patterns as the extinction map based on $H-Ks$ colors. Note that details will be more reliable in the map based on $H-Ks$ because of the higher point source desnity measured in these bands. Based on the assumption that the extinction law between Ks and L' is a power-law, we determined the corresponding power-law index, $\alpha_{Ks-L'}$, by requiring that the average A_{Ks} must be the same, based on $H-Ks$ or $Ks-L'$ colors. A value of $\alpha_{Ks-L'} = 1.35$ has been obtained, with a statistical uncertainty of 0.12 and a systematic uncertainty – due to uncertainties in the effective wavelengths and overall photometric calibration – of 0.29.

A histogram of the values of A_{Ks} measured based on the $H-Ks$ colors is shown in Fig. 7. The histogram is fit well by a Gaussian with a mean value of $A_{Ks,mean} = 2.71$ mag and a standard deviation of 0.30 mag.

The extinction map was used to produce an extinction corrected color magnitude diagram of Ks vs. $H-Ks$. It is shown in Fig. 8. It can be seen how the extinction correction significantly reduces the scatter in the diagram (compare with the uncorrected diagram in the upper left panel of Fig. 4). The red clump is very well defined and the giant sequence can be perceived clearly to the right of the dashed line, which indicates the median $H-Ks$ color. Stars on the left of the dashed line are expected to be either foreground or early-type stars. After exluding all stars with $H-Ks < 1.8$ mag as foreground and $H-Ks > 2.8$ as background stars, we have marked all stars with $Ks < 15$ and a color bluer than the median $H-Ks$ and redder than median $H-Ks-0.2$ mag (in order to exclude foreground stars) with crosses in the Ks image shown in Fig, 1. Many early-type stars reported by Paumard et al. (2006); Buchholz et al. (2009); Lu et al. (2009) and other authors are correctly identified. The method is rather crude and we estimate that of the order 30% of the stars may be spurious identifications and a similar number of early-type stars may be missed by this method. Nevertheless, this is the first time that early-type stars at the GC can be identified via broad-band imaging. Even taking into account the large estimated uncertainties, this rather crude method appears to confirm the finding of Buchholz et al. (2009) that there exists a population of early-type stars beyond a projected radius of 0.5 pc from Sagittarius A*.

Finally, we have used the extinction map to produce an extinction corrected Ks luminosity function (fore- and background stars excluded). It is shown in Fig. 9. It shows that in the shallow observations used in this work (in order to avoid saturating the brightest stars) the completeness drops below 50% already at $Ks \approx 17$.

6. Discussion

For comparison of the derived photometry and extinction with other work, it is important to refer to an effective wavelength, i.e. to take into account such factors as the SED of the stars, extinction, and the filter transmission curves. The measured value of the exponent of the power-law extinction-law is strongly dependent on the effective wavelength (see, e.g., Nishiyama et al. 2006a; Gosling et al. 2009; Stead & Hoare 2009). The transmission curves of the NACO filters are available at the ESO website. In order to facilitate comparison of our work, we have calculated

the effective wavelengths for the photometry presented here, using equation (A3) of Tokunaga & Vacca (2005).

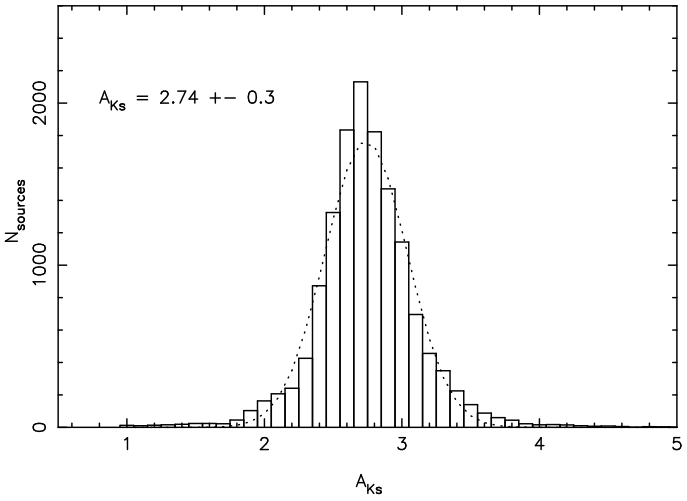

Fig. 7. Histogram of the extinction, A_{Ks}, based on $H - Ks$ colors.

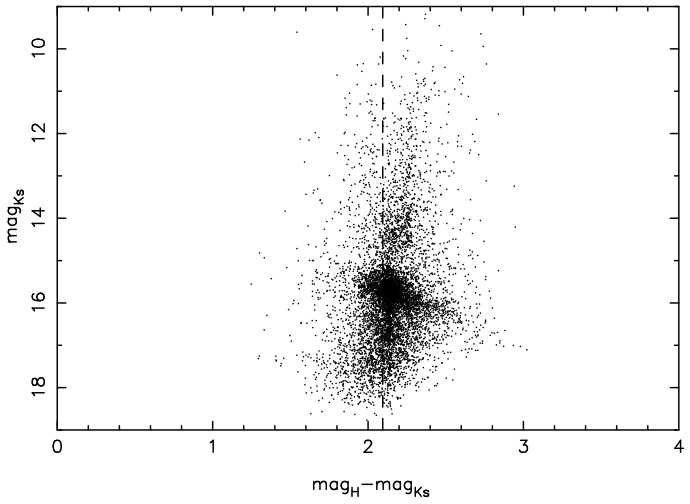

Fig. 8. Extinction corrected color-magnitude diagram for the GC. The dashed line indicates the mean $H - Ks$ color.

We have found a significantly steeper extinction law at NIR wavelengths than in earlier work (e.g., Rieke & Lebofsky 1985; Draine 1989; Mathis 1990, see the latter paper for a review). There exists, however, very agreement between the values for $\alpha_{H-Ks} = 2.22 \pm 0.23$ (and $\alpha_{H-Ks} = 2.54 \pm 0.15$, respectively) and $\alpha_{Ks-L'} = 1.38 \pm 0.29$ (and $\alpha_{Ks-L'} = 1.35 \pm 0.31$, respectively) found in this work and the respective values from other recent research. Gosling et al. (2009) report $\alpha_{J-Ks} = 2.64 \pm 0.52$ based on NIR observations of the nuclear bulge. Note that they find variability of this power-law index along the line-of-sight, on scales as small as 5". We have not examined spatial variability of the power-law index in our work. Since we do not have J-band observations available, we cannot determine the extinction-law toward individual stars or small groups of stars. Nishiyama et al. (2009) find $\alpha_{H-Ks} = 2.0$ and $\alpha_{Ks-3.6} = 1.37$, also based on NIR observations of the Galactic nuclear bulge. Stead & Hoare (2009) examined 8 regions from the UKIDDS Galactic Plane Survey and found $\alpha_{\rm NIR} = 2.14 \pm 0.05$. These values agree with

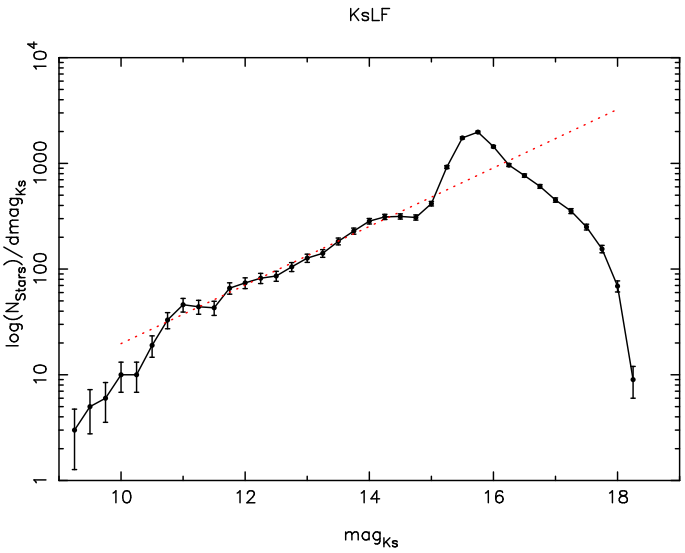

Fig. 9. Extinction corrected Ks luminosity function for the GC, fore- and background stars excluded. The red dashed line is a power law fit to the stars $11 < Ks < 14$. It has a power-law index of 0.27 ± 0.02.

our results within the 1σ - combined statistical and systematic - uncertainties. An exception is the value $\alpha_{H-Ks} = 2.54 \pm 0.15$ determined from the color dependence dependence of the RC in the $H - Ks$ vs. Ks color-magnitude diagram. Nevertheless, this error lies within the 1σ uncertainty of the value $\alpha_{H-Ks} = 2.22 \pm 0.23$ that we have derived in this work from the RC positions in the Ks and H luminosity functions. We consider the latter value more trustworthy because it is more straightforward to determine (no cutting out of regions from the color-magnitude diagram) and agrees very well with the other recent work cited above.

The extinction map based on $H - Ks$ colors presented in this work resembles closely the one presented in Buchholz et al. (2009). The overall extinction we find in this work is, however, lower than the one reported by Buchholz et al. (2009) – $A_{Ks} = 2.74 \pm 0.30$ compared to $A_{Ks} = 3.14 \pm 0.43$. The reason for this difference is the assumption of a flatter extinction law (based on Draine 1989) in Buchholz et al. (2009). The extinction map presented by Schödel et al. (2007a) is also similar to the one presented here, but shows a smaller FOV and is also based on a different extinction law. Agreement can also be seen between the extinction map produced in this work and the one presented by Scoville et al. (2003). The map in the latter paper encompasses a much larger region, but is less homogeneous than the one produced here because it is derived from the line emission of ionized gas. Due to the strong radio emission from Sagittarius A* the latter authors could not reliably constrain the extinction toward in the immediate surroundings of Sagittarius A*. Scoville et al. (2003) used an extinction-law of the form $A_\lambda \propto \lambda^{-.16}$, significantly different from what is found in this and other recent work on this subject.

A caveat may apply to the regions with the strongest extinction. As can be seen in Fig. 1, there are some regions (e.g. at an offset of $\sim +12$" E and ~ -13" S of Sagittarius A*) with very high extinction and consequently few stars. Extinction may be under-estimated by our method in these patches of extremely high extinction because the number of stars that can be detected behind a strong extinction screen may be very small.

Finally, useful for analyses of the so-called "S-cluster" of stars that are tightly bound to Sagittarius A* and of the NIR emission of Sgr A* itself, we can use the extinction map pre-

sented in Fig. 6 to calculate the mean extinction and its standard deviation toward Sagittarius A*. For a circular region with a radius of 0.5" centered on Sagittarius A* we obtain $A_{H,SgrA*} = 4.34 \pm 0.11$, $A_{Ks,SgrA*} = 2.45 \pm 0.03$, and $A_{L',SgrA*} = 1.24 \pm 0.08$. The uncertainties for $A_{H,SgrA*}$ and $A_{L',SgrA*}$ include the uncertainties of α_{H-Ks} and $\alpha_{Ks-L'}$. These values are different from values that have typically been used in the analysis of NIR lightcurves from Sgr A*, e.g., $A_H = 4.3$, $A_K = 2.8$, $A_{L'} = 1.8$ (Genzel et al. 2003; Eckart et al. 2006), $A_K = 3.3$ (Do et al. 2009), or $A_{L'} = 1.8$ (Ghez et al. 2004). While the impact on emission/accretion models of Sgr A* will probably be minor, we point out that the new extinction values at Ks and L' imply that the de-reddened emission from Sgr A* may be weaker than assumed by a factor $1.4 - 2.2$ at Ks and a factor of ~ 1.7 at L'.

A correct estimate of the extinction is crucial to address one of the long standing issues in the central parsec, namely the apparent incompatibility between the ionizing flux arising from the massive stars and the ionisation of the gas (Najarro et al. 1997b; Lutz 1999). Further, these authors found that the population of HeI stars, displaying fairly large luminosities was unusually high. Such incompatibility was recently claimed to be solved by Martins et al. (2007b) with the inclusion of line-blanketing in the models, leading to lower bolometric luminosities and lower UV fluxes for the HeI stars. However, we attribute most of the discrepancy between the results of Najarro et al. (1997b) and Martins et al. (2007b) for the HeI stars to the estimate of A_K between both investigations. Indeed, the final A_K values computed by Najarro et al. (1997b) were 50% larger than the ones adopted by Martins et al. (2007b) from the extinction map of Schödel et al. (2007a). Such difference was translated into roughly one magnitude in luminosity and was responsible for the much lower luminosity of the HeI stars revised by Martins et al. (2007b). Similarly, the nature of the "S" stars is also affected. While Martins et al. (2008) adopted $A_K = 2.25$ for S2 it turns out that the extinction map they used was calibrated on S2 with an $A_K = 2.8$ Schödel et al. (2007a). That would have changed S2 from being a dwarf to being a giant. It turns out that the actual value of $A_{Ks} = 2.45$ toward S2 is not too different from the value assumed (erroneously) by Martins et al. (2008). As we show in this work, and as other similar recent investigation has shown, the solution and key to these problems is that the power-law slope of the NIR extinction law is significantly steeper than what was assumed in earlier work. This leads to lower extinction in the K-band, but significantly stronger extinction at shorter wavelengths.

In Fig. 10 we show a color composite image of the stars, detected at Ks, the A_{Ks} extinction, and the MIR (PAH I) emission (data from Schödel et al. 2007b). It can be seen how the extinction is low in a region running roughly from SW to NE. This creates an apparent high stellar density and therefore elongation of the NSC along the galactic plane (as was also shown by Schödel et al. 2007a). Similarly, the lower extinction to the NW of Sgr A* is responsible for the higher stellar density observed in that region. The strong influence that extinctino has on the appearance of the nuclear star cluster can also be nicely seen in Fig. 1 of Scoville et al. (2003). There appears to be no obvious relation between the warm dust emitting in the mid-infrared and the extinction. This is no surprise because the surface density of HI and H_2 and the warm dust associated with it in the mini-spiral is just of the order a few $\times 10^4$ cm^{-3}(see, e.g., discussion of this topic in Moultaka et al. 2009). The extinction toward the GC is largely produced by clouds in the foreground, with the possible exception of some dust-enshrouded individual objects (Moultaka et al. 2009) .

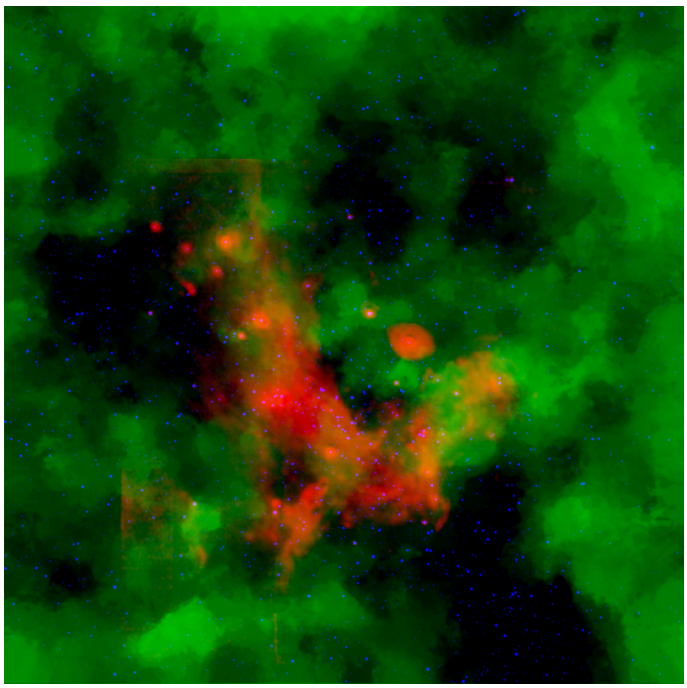

Fig. 10. Ilustration of the relation between the stars detected at Ks (blue), the A_{Ks} extinction (green), and the diffuse emission in the mid-infrared (PAH I, red).

We believe that future work should focus on deriving the power-law index for the NIR extinction-law toward the GC with higher precision and examine its variability over the central parsecs. This could be achieved, for example, by deep AO imaging using a large number of narrow band filters across the near-infrared. The main limitation for this kind of work may come from the still limited performance of AO systems at short NIR wavelengths (J-band), combined with the long exposure times required by the high extinction. An additional great difficulty, in fact the main source of uncertainty in this work, is the difficulty to obtain precise and accurately calibrated photometry from AO data (crowding, large seeing foot of PSF, spatial variability of PSF). We have, however, no doubt that there will be significant technical progress in AO techniques and related data processing software in the next few years.

7. Summary

We provide photometry for ~ 7700 point sources extracted from adaptive optics observations of the central parsec of the Galactic center in the H, Ks, and L' bands. The data are made publicly available. Adaptive optics photometry has been published previously in some papers. However, we believe that the data presented in this work supersede those earlier results or are complementary to them because of reasons such as: (a) limited field-of-view of previous observations or focus on the central few 0.1 pc; (b) isoplanatic effects were not taken properly into account; (c) bias by the application of methods such as Lucy-Richardson deconvolution (the companion paper to this work, by Schoedel submitted to A&A, explains our photometric method and points out the bias introduced by the Lucy-Richardson method); (d) no transparent explanation of the photometric calibration. This data set is the most comprehensive one published so far.

Based on the photometric results, we analyze extinction toward the central parsec of the GC. Absolute values of extinction in the three examined bands are derived based on the well-known

properties of red clump stars, without the need to measure stellar colors and without having to assume an extinction law. The values obtained are $A_H = 4.46 \pm 0.12$ mag, $A_{Ks} = 2.52 \pm 0.12$ mag, and $A_{L'} = 1.24 \pm 0.18$ mag. This results in $A_H : A_{Ks} : A_{L'} = 1.77 : 1 : 0.49$. Assuming the validity of a power-law extinction law between H and Ks and between Ks and L', this is equivalent to power-law indices of $\alpha_{H-Ks} = 2.22 \pm 0.23$ and $\alpha_{Ks-L'} = 1.38 \pm 0.29$. This is significantly steeper than in earlier work (e.g. Rieke & Lebofsky 1985; Draine 1989), but agrees with recent studies of extinction toward the nuclear bulge (Nishiyama et al. 2009; Gosling et al. 2009) and other targets in the Galactic plane (Stead & Hoare 2009). We also confirm the flattening of the extinction law beyond $\sim 3\,\mu$m (see also Lutz et al. 1996; Indebetouw et al. 2005; Viehmann et al. 2005; Flaherty et al. 2007; Nishiyama et al. 2009).

Based on $H - Ks$ colors of the stars, we provide a detailed, accurate extinction map for a FOV of 40"×40" (~ 1.5 pc×1.5 pc) centered roughly on Sagittarius A*. The spatial resolution of the map is $\sim$ 1". Both statistical and systematic uncertainties of the extinction map are lower than 10%. We find that extinction varies significantly on arcsecond scales. The mean extinction based on stellar colors is found to be $A_{Ks} = 2.74 \pm 0.30$ mag, in good agreement with the value of mean extinction based on the RC method. An extinction map based on $Ks - L'$ colors, although less accurate because of lower point source surface density and possible contamination by diffuse emission from dust in the mini-spiral, confirms the patterns seen in the extinction map based on $H - Ks$ colors. Requiring the mean extinction between the two maps to be the same, we derive $\alpha_{Ks-L'} = 1.35 \pm 0.31$, in excellent agreement with the value of this parameter derived from the mean magnitudes of the RC bump (see above).

Applying the derived extinction law and the measured absolute extinction to the observed $H - Ks$ colors of the stars, we are able to correct the corresponding color-magnitude diagram. This reduces the scatter in this diagram considerably and makes it possible, for the first time, to distinguish the giant and the main sequence branches in such a diagram for the GC. We confirm recent findings of the presence of a pouplation of young, massive stars are present at projected distances > 0.5 pc from Sagittarius A*.

A minor, but very interesting by-product of this work is a weighted average of recent (years 2006-2009) estimates of R_0. We find that the distance of the GC is constrained with an uncertainty of just 2%: $R_0 = 8.04 \pm 0.16$ kpc.

For a circular region with a radius of 0.5" centered on Sagittarius A* we obtain $A_{H,SgrA*} = 4.34 \pm 0.11$, $A_{Ks,SgrA*} = 2.45 \pm 0.03$, and $A_{L',SgrA*} = 1.24 \pm 0.08$. These values imply that the NIR emission from Sgr A* in the Ks and L'-bands may be weaker than previously assumed, by factors 1.4 – 2.3.

We have used the following effective wavelengths in this work: $\lambda_H = 1.677 \pm 0.012\,\mu$m, $\lambda_{Ks} = 2.168 \pm 0.012\,\mu$m, and $\lambda_{\rm eff,L'} = 3.636 \pm 0.012\,\mu$m. Note that the effective wavelength is a complex function of the transmission functions of the atmosphere, the filter, the optical system, extinction, and stellar type. For discussions of this problem, see, for example, Espinoza et al. (2009) and Stead & Hoare (2009). The uncertainties cited for the effective wavelengths are based on best-estimates of the variablity of these values for the case of Galactic center observations and the observing conditions and instruments used in this work.

Acknowledgements. RS acknowledges the Ramón y Cajal programme of the Spanish Ministerio de Ciencia e Innovación (MICINN) and support by the MICINN project AYA2007-64052.

References

Alves, D. R. 2000a, ApJ, 539, 732
Alves, D. R. 2000b, ApJ, 539, 732
Bartko, H., Martins, F., Fritz, T. K., et al. 2009, ApJ, 697, 1741
Böker, T. 2008, Journal of Physics Conference Series, 131, 012043
Buchholz, R. M., Schödel, R., & Eckart, A. 2009, ArXiv e-prints, 499, 483
Castellani, V., Chieffi, A., & Straniero, O. 1992, ApJS, 78, 517
Cox, A. N. 2000, Allen's astrophysical quantities, ed. A. N. Cox
Devillard, N. 1997, The Messenger, 87, 19
Diolaiti, E., Bendinelli, O., Bonaccini, D., et al. 2000, in Society of Photo-Optical Instrumentation Engineers (SPIE) Conference Series, Vol. 4007, Society of Photo-Optical Instrumentation Engineers (SPIE) Conference Series, ed. P. L. Wizinowich, 879–888
Do, T., Ghez, A. M., Morris, M. R., et al. 2009, ApJ, 691, 1021
Draine, B. T. 1989, in ESA Special Publication, Vol. 290, Infrared Spectroscopy in Astronomy, ed. E. Böhm-Vitense, 93–98
Eckart, A., Baganoff, F. K., Schödel, R., et al. 2006, A&A, 450, 535
Espinoza, P., Selman, F. J., & Melnick, J. 2009, A&A, 501, 563
Flaherty, K. M., Pipher, J. L., Megeath, S. T., et al. 2007, ApJ, 663, 1069
Genzel, R., Schödel, R., Ott, T., et al. 2003, Nature, 425, 934
Ghez, A. M., Salim, S., Weinberg, N. N., et al. 2008, ApJ, 689, 1044
Ghez, A. M., Wright, S. A., Matthews, K., et al. 2004, ApJ, 601, L159
Gillessen, S., Eisenhauer, F., Trippe, S., et al. 2009, ApJ, 692, 1075
Gosling, A. J., Bandyopadhyay, R. M., & Blundell, K. M. 2009, MNRAS, 394, 2247
Gosling, A. J., Blundell, K. M., & Bandyopadhyay, R. 2006, ApJ, 640, L171
Grocholski, A. J. & Sarajedini, A. 2002, AJ, 123, 1603
Groenewegen, M. A. T. 2008, A&A, 488, 935
Groenewegen, M. A. T., Udalski, A., & Bono, G. 2008, A&A, 481, 441
Indebetouw, R., Mathis, J. S., Babler, B. L., et al. 2005, ApJ, 619, 931
Lord, S. 1992, Tech. rep.
Lu, J. R., Ghez, A. M., Hornstein, S. D., et al. 2009, ApJ, 690, 1463
Lutz, D. 1999, in ESA Special Publication, Vol. 427, The Universe as Seen by ISO, ed. P. Cox & M. Kessler, 623–+
Lutz, D., Feuchtgruber, H., Genzel, R., et al. 1996, A&A, 315, L269
Maness, H., Martins, F., Trippe, S., et al. 2007, ApJ, 669, 1024
Martins, F., Genzel, R., Hillier, D. J., et al. 2007a, A&A, 468, 233
Martins, F., Genzel, R., Hillier, D. J., et al. 2007b, A&A, 468, 233
Martins, F., Gillessen, S., Eisenhauer, F., et al. 2008, ApJ, 672, L119
Mathis, J. S. 1990, ARA&A, 28, 37
Matsunaga, N., Kawadu, T., Nishiyama, S., et al. 2009, ArXiv e-prints
Moultaka, J., Eckart, A., & Schödel, R. 2009, ArXiv e-prints
Najarro, F., Krabbe, A., Genzel, R., et al. 1997a, A&A, 325, 700
Najarro, F., Krabbe, A., Genzel, R., et al. 1997b, A&A, 325, 700
Nishiyama, S., Nagata, T., Baba, D., et al. 2005, ApJ, 621, L105
Nishiyama, S., Nagata, T., Kusakabe, N., et al. 2006a, ApJ, 638, 839
Nishiyama, S., Nagata, T., Sato, S., et al. 2006b, ApJ, 647, 1093
Nishiyama, S., Nagata, T., Tamura, M., et al. 2008, ApJ, 680, 1174
Nishiyama, S., Tamura, M., Hatano, H., et al. 2009, ApJ, 696, 1407
Paumard, T., Genzel, R., Martins, F., et al. 2006, ApJ, 643, 1011
Reid, M. J., Menten, K. M., Zheng, X. W., et al. 2009, ArXiv e-prints
Rieke, G. H. & Lebofsky, M. J. 1985, ApJ, 288, 618
Schödel, R., Eckart, A., Alexander, T., et al. 2007a, A&A, 469, 125
Schödel, R., Eckart, A., Mužić, K., et al. 2007b, A&A, 462, L1
Schoedel, R., Merritt, D., & Eckart, A. 2009, ArXiv e-prints
Scoville, N. Z., Stolovy, S. R., Rieke, M., Christopher, M., & Yusef-Zadeh, F. 2003, ApJ, 594, 294
Seth, A. C., Blum, R. D., Bastian, N., Caldwell, N., & Debattista, V. P. 2008, ApJ, 687, 997
Stead, J. J. & Hoare, M. G. 2009, ArXiv e-prints
Sumi, T. 2004, MNRAS, 349, 193
Tokunaga, A. T. & Vacca, W. D. 2005, PASP, 117, 421
Trippe, S., Gillessen, S., Gerhard, O. E., et al. 2008, A&A, 492, 419
Udalski, A. 2003, ApJ, 590, 284
Viehmann, T., Eckart, A., Schödel, R., et al. 2005, A&A, 433, 117
Wozniak, P. R. & Stanek, K. Z. 1996, ApJ, 464, 233

Appendix A: Effective wavelength

We calculated the effective wavelengths of our observations following equation (A3) of Tokunaga & Vacca (2005). The transmission curves for the NACO H and Ks filters were downloaded from the instrument web site[2]. Spectra of the atmospheric trans-

[2] http://www.eso.org/sci/facilities/paranal/instruments/naco/index.html

mission were downloaded from the Gemini telescope web site[3]. They are based on models with the ATRAN software (Lord 1992). The transmission curves for 3 mm precipitable water vapor were used because humidity was high during the H and Ks observations.

We did not use any particular stellar atmosphere model for the calculations. Instead, simple extincted blackbody models were used. Table A.1 lists the values of the effective wavelength for various values of A_K and effective temperatures of the blackbodies. A power-law $A_K \propto \lambda^{-\alpha}$ (Nishiyama et al. 2009) was used to calculate the extinction at different wavelengths. We assumed $\alpha_{H-Ks} = 2.22$ for the extinction between H and Ks , and $\alpha_{Ks-L'} = 1.33$ for the extinction between Ks and L' [4]. The majority (> 90%) of stars in the images analyzed in this work are of late-type, with a large percentage of RC stars (see, e.g., Buchholz et al. 2009). We therefore adopt as effective wavelengths $\lambda_{\rm eff,H} = 1.677\,\mu$m, $\lambda_{\rm eff,Ks} = 2.168\,\mu$m, and $\lambda_{\rm eff,L'} = 3.636\,\mu$m for an average extinction of $A_{KS} \approx 2.5$.

The uncertainty introduced by the choice for the amount of precipitable water vapor is low. Choosing 1.6 mm instead of 3.0 mm will change the effective wavelengths by $\leq 0.003\,\mu$m for H, $\leq 0.001\,\mu$m for Ks, and $\leq 0.01\,\mu$m for L'. Changing the power-law index for the extinction curve between H and Ks to $\alpha_{H-Ks} = 2.0$ (Nishiyama et al. 2009) results in a change of $\leq 0.003\,\mu$m for $\lambda_{\rm eff,Ks}$, and $\leq 0.009\,\mu$m for $\lambda_{\rm eff,H}$. Changing the power-law index for the extinction curve between Ks and L' to $\alpha_{Ks-L'} = 1.37$ (Nishiyama et al. 2009) results in a change of $< 0.001\,\mu$m for $\lambda_{\rm eff,L'}$. The uncertainty in extinction introduces an uncertainty of $\lesssim 0.015\,\mu$m for H, $\lesssim 0.01\,\mu$m for Ks, and $\lesssim 0.002\,\mu$m for L'. The unknown effective temperature of the stars introduces uncertainties of $\lesssim 0.005\,\mu$m for H, $\lesssim 0.006\,\mu$m for Ks, and $\lesssim 0.001\,\mu$m for L'.

We estimate the combined $1\,\sigma$ uncertainty of the effective wavelengths to $0.018\,\mu$m for H, $0.012\,\mu$m for Ks, and $0.012\,\mu$m for L'.

Table A.1. Effective wavelengths in units of μm for the NACO H, Ks, and L' filters for blackbodies with different effective temperatures and extinction. The effective temperature is given in the left column, the extinction A_{Ks} in the first line of the table.

H				
	2.0	2.5	3.0	3.5
3000	1.674	1.681	1.688	1.695
4700	1.669	1.677	1.684	1.691
30000	1.664	1.672	1.680	1.687
Ks				
3000	2.167	2.171	2.176	2.180
4700	2.163	2.168	2.173	2.177
30000	2.159	2.164	2.169	2.174
L'				
3000	3.636	3.637	3.638	3.639
4700	3.635	3.636	3.637	3.638
30000	3.634	3.635	3.636	3.637

[3] http://www.gemini.edu/node/10781?q=node/10789

[4] This value of $\alpha_{Ks-L'}$ is from a preliminary estimate at the beginning of this work and is smaller than the value $\alpha_{Ks-L'} = 1.38$ that we derived in the end. However, the associated change of $\lambda_{\rm eff,L'}$ is minimal, see discussion of the uncertainties in the next paragraph.

Table A.2. List of detected point sources in the H, Ks, and L'-band observations. Coordinates are given as offsets from Sgr A*. Uncertainties in the astrometric positions can be as large as ~ 0.1" because high precision astrometry was not at the focus of this work. The conversion to offsets from Sgr A* was done by assuming a pixel scale of 0.027" per pixel (ESO NACO manual). The camera rotation angle was assumed 0 deg east of north and no camera distortion solution was applied. The second column gives the projected distance from Sgr A* in arcseconds. We only include the first ten lines of the table in the printed edition of this work. The photometric uncertainties include formal uncertainties from PSF fitting, based on Gaussian read-out noise and Poisson photon noise, and the uncertainties due to the limited knowledge of the PSF. The $1\,\sigma$ uncertainties of the zero points are not included. They are $\Delta ZP_H = 0.06$, $\Delta ZP_{Ks} = 0.06$, and $\Delta ZP_{L'} = 0.15$. The uncertainty of the zero points includes both the original uncertainty of the ESO zero point and its additional uncertainty introduced by the PSF used for Wiener deconvolution of the images prior to PSF fitting (both uncertainties were quadratically combined). A value of 0.0 in the table indicates that the corresponding measurement is not available.

ID	R_{SgrA*} ["]	R.A. ["]	Dec. ["]	H	ΔH	Ks	ΔKs	magL'	$\Delta L'$
1	0.028	0.009	-0.027	17.50	0.05	15.7	0.04	0.0	0.0
2	0.107	0.031	-0.102	18.19	0.06	16.39	0.04	0	0
3	0.163	-0.006	0.163	16.00	0.02	14.13	0.01	12.84	0.03
4	0.231	0.189	0.132	16.93	0.03	15	0.01	0	0
5	0.245	-0.231	-0.081	18.69	0.07	16.75	0.05	0	0
6	0.265	0.022	-0.264	16.53	0.03	14.7	0.02	0	0
7	0.321	0.296	0.124	16.47	0.02	14.61	0.01	0	0
8	0.347	-0.274	0.213	17.45	0.03	15.66	0.09	14.35	0.06
9	0.354	-0.053	0.35	17.22	0.03	15.39	0.02	0	0
10	0.363	0.02	-0.363	16.23	0.03	14.12	0.01	12.6	0.03